Physics of the Earth and Planetary Interiors, 47 (1987) 188–204
Elsevier Science Publishers B.V., Amsterdam – Printed in The Netherlands

Stacking investigations of the dispersion of higher order mantle Rayleigh waves and normal modes

Emile A. Okal and Bong-Gon Jo *

Department of Geological Sciences, Northwestern University, Evanston, IL 60201 (U.S.A.)

(Received December 31, 1985; revision accepted October 1, 1986)

Okal, E.A. and Jo, B.-G., 1987. Stacking investigations of the dispersion of higher order mantle Rayleigh waves and normal modes. Phys. Earth Planet. Inter., 47: 188–204.

Using a number of stacking techniques (including non-linear stacking), we have systematically investigated, both in the travelling wave and normal mode formalisms, the dispersion of the third, fourth and fifth branches of Rayleigh overtones, which travel with identical group velocities at similar frequencies, and are a prominent part of the horizontal, away from the source, components of long-period seismograms from major earthquakes. Using data from six major events recorded on the Global Digital Seismological Network, we have extracted more than 100 normal modes from these three branches in the period range 82–160 s; our results are generally in excellent agreement with values computed from available models of the Earth, and also with previously published values for a well-separated part of the third branch.

1. Introduction

Because their eigenfunctions sample the Earth deeper than fundamentals of similar periods, surface-wave overtones have long been a target of interest by scientists investigating the Earth's crust and upper mantle. Kovach and Anderson (1964) used Rayleigh overtones in the 5–50 s range to study the oceanic low-velocity zone; later Nolet (1975, 1977) identified up to the 6th overtone in the 20–50 s range under Europe, Cara (1978) and Cara et al. (1980) used mostly the 1st and 2nd overtones, ${}_1R$ and ${}_2R$, in the 30–70 s range to investigate lateral heterogeneity under the Pacific, North America and Eurasia, and Okal and Jo (1983) regionalized the dispersion of prominent ${}_1R$ phases from deep earthquakes in the 70–150 s range. Most such studies involved the vertical component of motion.

* Also at the Department of Geology and Geophysics, Yale University, Box 6666, New Haven, CT 06511, U.S.A. Present address: Department of Geology, Jeonbug National University, Jeonju, Jeonbug 520, Republic of Korea.

In the 80–150 s range, the 3rd, 4th, and 5th Rayleigh overtones ${}_3R$, ${}_4R$, ${}_5R$, can be substantially excited by earthquake sources in the 30–450 km depth range. This theoretical result is shown in Fig. 1, which compares the excitability of the first six branches of Rayleigh modes around 100 s. We define the vertical excitability of the mode as

$$E_v = \sqrt{K_0^2/4l + lK_1^2 + l^3K_2^2} \quad (1)$$

where K_0, K_1, K_2 are excitation coefficients in the formalism of Kanamori and Stewart (1976). At any given frequency and depth, E_v represents an estimate of the excitation of a given overtone surface wave by a double-couple of unknown geometry. Because the 3rd, 4th, and 5th overtones are characterized by extremely flat aspect ellipses at the surface, we also consider the horizontal excitability

$$E_h = l\,|\,y_3\,|\,E_v \quad (2)$$

where y_3 is the amplitude of the horizontal function at the Earth's surface, the vertical eigenfunction y_1 being normalized at the surface. Figure 1

0031-9201/87/$03.50

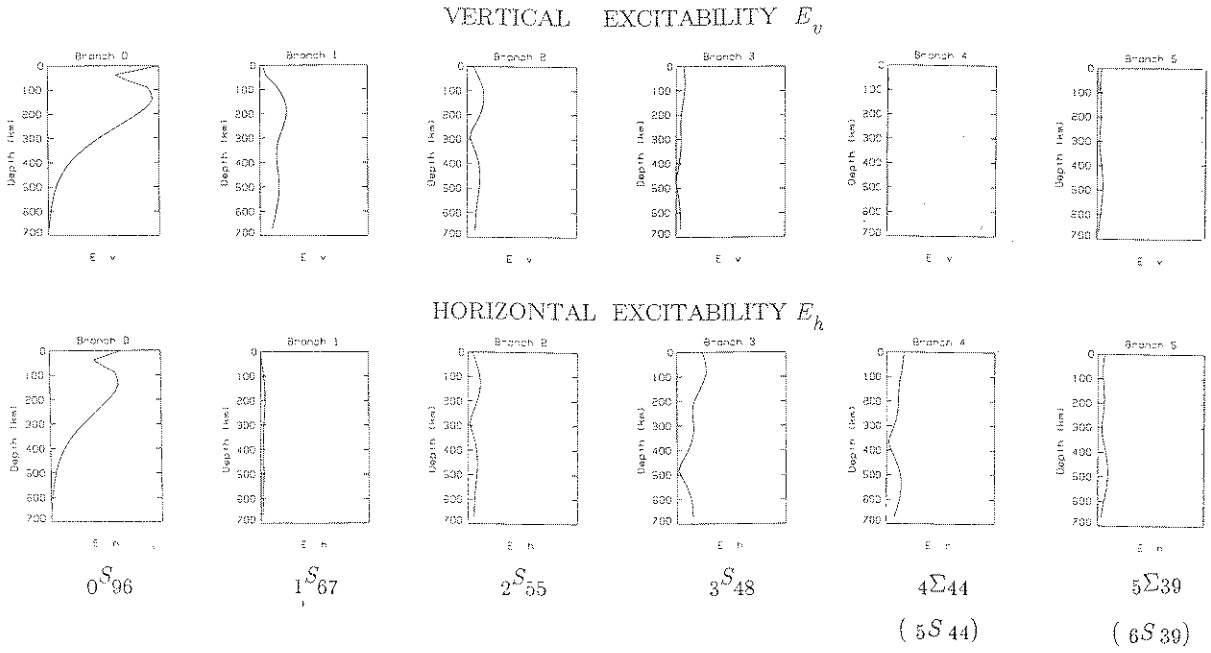

Fig. 1. Excitability of the first six Rayleigh branches plotted as a function of depth. The modes all have a period close to 100 s. See text for definition of E_v and E_h. The horizontal scales are arbitrary, but common to all 12 diagrams. Note the strong horizontal excitability of the third and fourth overtones around 100 s. The notation $_p\Sigma_l$ is explained in section 3.

clearly shows that these overtones, especially the 3rd one, can substantially contribute to horizontal motion for sources as shallow as 50 km, in contrast in particular to the first overtone, whose aspect ellipse is practically vertical at similar periods (as the period is decreased towards 80 s, the influence of the 4th, and then 5th branches becomes preponderant at the expense of the 3rd overtone). As a result, the radial (away from the source) components of long-period or broad-band seismograms from major earthquakes prominently exhibit the successive passages of the corresponding Rayleigh waves (Fig. 2). This was first recognized by Jobert et al. (1977) who referred to the wave as 'phase X', and to its q-th passage as X_q. Jobert (1978) later synthetized it as a sum of mantle overtones principally from the branches $_3R$, $_4R$, $_5R$.

While in certain instances, it appears that each passage X_q can be decomposed into the individual wavetrains $_pR_q$ for each branch p, this becomes clearly impossible in many situations. For example, in Fig. 2, the phase X_3 continuously rings between 22:01:30 and 22:17:00 GMT, corresponding to group arrivals between 6.4 and 5.75 km s^{-1}, while X_4 is characterized by well separated arrivals at 22:35 (6.44 km s^{-1}), 22:44 (6.11 km s^{-1}), and 22:50 (5.92 km s^{-1}).

This is due to the fact that group velocity curves for $_3R$, $_4R$, and $_5R$ feature inverse dispersion and considerable overlap at velocities of 5.8–6.6 km s^{-1}. Further, and as shown in Fig. 3, the details of this overlap are strongly model dependent: merely going from a young ocean to an old ocean model can increase the group velocity of $_3R$ by as much as 0.3 km s^{-1}, and move its overlap with $_4R$ from 130 to 110 s.

Despite these difficulties, the resolving kernels of overtones inside the upper mantle are clearly different from those of fundamentals, and thus hold promise for increased resolving power in the inversion of structural characteristics (both global and local) from seismic wave data. The aim of this study is to describe methods of extraction of individual overtone branches, and to present an extensive dataset of their dispersion.

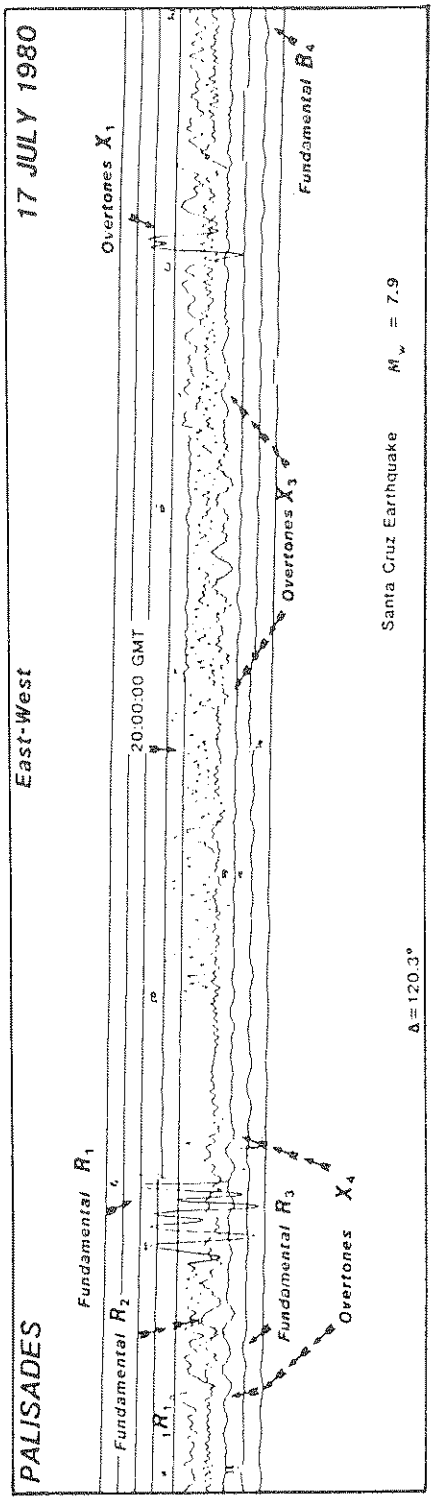

Fig. 2. East–west (away from the source) long-period seismogram of the 1980 Santa Cruz earthquake at Palisades, NY, showing the first four passages of the fundamental Rayleigh wave R, and of the overtone wavetrain X. The second passage X_2 is lost in the signal of the fundamental R_1, which goes off-scale. Each trace is 1 h long.

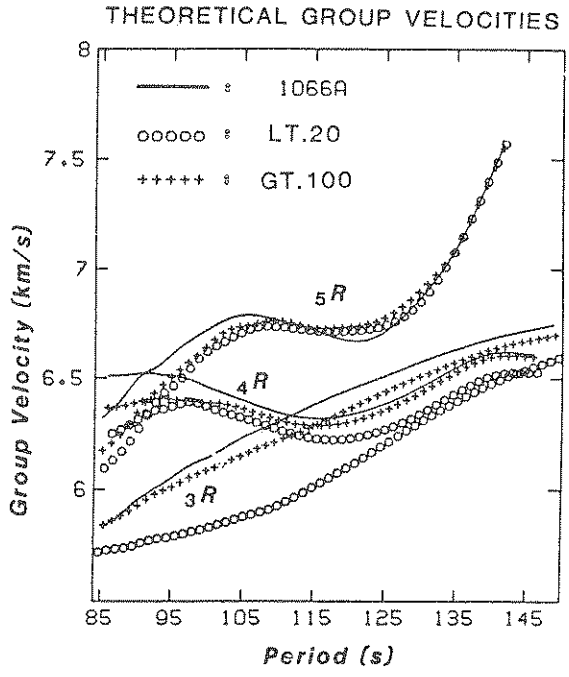

Fig. 3. Theoretical group velocity dispersion curves of the branches $_3R$, $_4R$, and $_5R$, computed for global model 1066A, and two oceanic models (young –LT.20 and old –GT.100; (Mitchell and Yu, 1980)). The details of the inverse dispersion are strongly model dependent, but in all cases, overlap occurs between $_4R$ and $_5R$ in the 90–100 s range, and between $_4R$ and $_3R$ in the 105–150 s range.

2. Travelling wave approach

2.1. Techniques

A classic method of extracting individual overtones from a complex seismogram is the so-called 'time variable filtering' described by Dziewonski et al. (1968) and Landisman et al. (1969). Its basic idea is to target different time windows of the seismogram at different frequencies, closely following an estimate of the group velocity dispersion curve of a given overtone. While this method has had considerable success in extracting Rayleigh overtones at higher frequencies, it fails to separate overtone branches travelling with similar group velocities at similar periods, such as those making up phase X. In this respect, it is interesting to note that Roult and Romanowicz (1984) extracted modes of the $_3R$ branch from records of the 1983 Costa Rica event, but only at periods less than 114 s. This is precisely the period where the branch is expected to start overlapping with $_4R$, according to the models in Fig. 3. We recover the longer period part of the branch in the course of this study.

Spatial filtering, involving stacking of records at several stations, can be used to refine the extraction of individual branches. This method, introduced by Nolet and Panza (1976) and Cara (1976), separates the modes by wavenumber, or equivalently *phase* velocity, and thus is insensitive to problems arising from overlap of group arrival times. Specifically, one uses records at a number of stations aligned with the epicenter, narrowly filtered around an angular frequency ω_0, and stacks them after correcting their phase for propagation using a trial phase velocity C_0 at frequency ω_0. By looping over C_0 and analyzing each stack with standard group velocity techniques, one maps the energy contained in the U–C plane. Cara [1978] used this method to efficiently separate the 1st and 2nd higher Rayleigh modes. We confirmed in a synthetic experiment that it has the potential to separate $_3R$, $_4R$, and $_5R$, provided an adequate dataset can be found. However, when dealing with higher overtones at very large wavelengths, and with the very few major earthquakes providing substantial excitation, it becomes increasingly difficult to identify a suitable alignment of stations.

To use the high-quality data from the sparser Global Digital Seismic Network (GDSN), we relax the constraint of alignment with the epicenter, and further correct for the azimuthal effect of the focal geometry on the initial phase. Specifically, at each angular frequency ω, the phase ϕ_j of the Fourier component $a_j(\omega)$ of horizontal ground motion at station j is given by

$$\phi_j(\omega) = \phi_0(\omega) - \frac{\pi}{4} + (q-1)\frac{\pi}{2} - \frac{\omega X_j}{C(\omega)} + \psi_j(\omega) \tag{3}$$

where ϕ_0 is due to the source time function, $C(\omega)$ is the true phase velocity of the mode averaged over the path to station j, X_j is the total length of this path, including ellipticity corrections (which become important when using stations on widely

differing great circles and large values of the order of passage q), and $\psi_j(\omega)$ is the phase of the excitation term $[s_R K_0 - l^2 p_R K_2 - i\ lq_R K_1]$ where $l = a\omega/C - 1/2$, the notation being that of Kanamori and Stewart (1976). ψ_j can be computed at all azimuths for a given focal mechanism and Earth model; its dependence on station azimuth and focal depth is much stronger than on the small variations in C which we are solving for.

To test the power of this method, we used it to retrieve the dispersion of the branches targeted in this study from synthetic seismograms. We used the Earth model 1066A (Gilbert and Dziewonski, 1975), and focal parameters reproducing the geometries of our real data. Figure 4 shows the result of this improved spatial filtering applied to a set of synthetic X_4 phases from nine stations, and stacked for the 4th overtone. The phase and group velocity are recovered within the precision of the mesh chosen in the U–C plane.

2.2. *Dataset and results*

Table I lists epicentral parameters of events used in this study; for the surface wave investigation, we used GDSN data from five large earthquakes (Events 2–6). Focal mechanisms, necessary for the computation of the ψ_j's, were taken from Kanamori and Given (1982), Romanowicz and Guillemant (1984), and the Harvard solutions (Dziewonski et al., 1983a,b). To prevent possible contamination of the records with fundamental wave energy, we eliminated all stations for which ${}_0R_q$ and X_p $(q < p)$ have similar group arrival times. In practice, this means rejecting all X_2 wavetrains which arrive in the coda of the prominent ${}_0R_1$, and working with X_p $(p = 3–6)$. We further eliminate those stations for which a particular ${}_0R_q$ $(q > 1)$ can contaminate these X phases. This leaves us with typically 8–10 SRO stations. We use time windows of 40 min duration, which in all cases span arrival times at group velocities of 5.8–6.6 km s^{-1}.

Figure 5 is an example of U–C diagrams of records of the 1980 Santa Cruz earthquake at 99.1 s, stacked for the 4th passage of, respectively, the 3rd and 4th overtones (this particular period was selected to match the mode ${}_3S_{49}$). This figure demonstrates the efficient separation of the two branches, and confirms the overlap in group veloc-

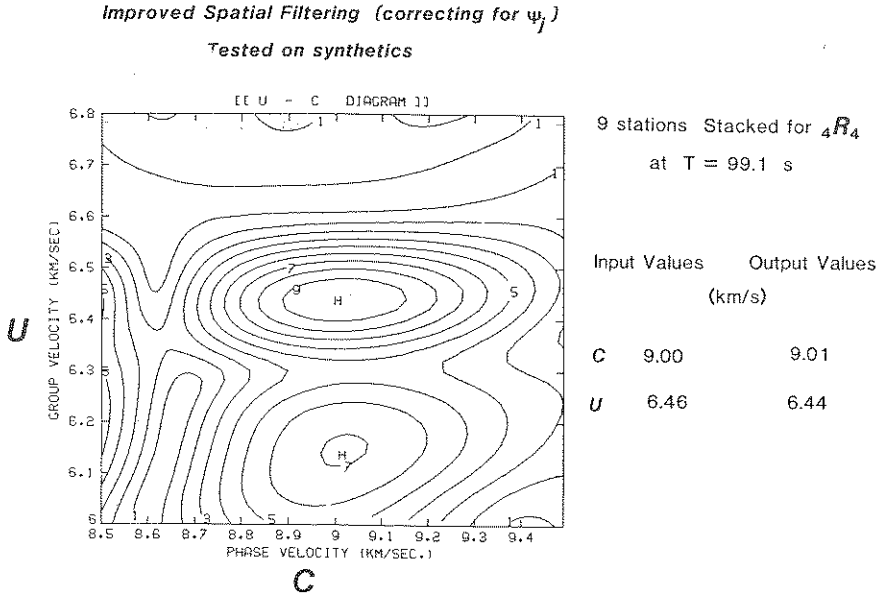

Fig. 4. Improved spatial filtering (correcting for the azimuthal phase ψ_j) tested on synthetics. The seismograms are computed at nine stations with varying source azimuths. The targeted branch, ${}_4R$, is recovered within the precision of the U–C mesh. Numbers on contours are decimal fractions of the maximum amplitude resulting from combining each stack with its Hilbert transform.

TABLE I

Epicentral and focal parameters of earthquakes used in this study

Event Number	Region	Date			Origin Time GMT	Epicenter		Depth (km)	Moment (10^{27} dyn-cm)	Focal mechanism *			
		Year	month	day		°N	°E			ϕ(°)	δ(°)	λ(°)	Reference
1	Colombia	1979	11	23	23:40:29.8	4.81	−76.22	110	0.8	150	45	219	a
2	Colombia	1979	12	12	07:59:04.4	1.62	−79.34	28	20	179	78	83	a
3	Santa Cruz	1980	07	17	19:42:23.2	−12.52	165.92	33	8	142	63	70	b
4	Banda Sea	1982	06	22	04:18:40.5	−7.34	126.04	450	2	310	70	225	c
5	New Ireland	1983	03	18	09:50:50.0	−4.88	153.58	85	6.7	49	54	79	a
6	Costa Rica	1983	04	03	02:50:01.1	8.72	−83.12	33	0.5	305	15	90	d

* Focal mechanism notations are those of Kanamori and Cipar (1974).

References to focal mechanisms are: (a) Romanowicz and Guillemant (1984); (b) Kanamori and Given (1982); (c) Dziewonski et al. (1983a); (d) Dziewonski et al. (1983b).

ity. Table IIa–c summarizes our results for the branches ${}_3R$, ${}_4R$ and ${}_5R$, obtained from fourth and sixth passage wave packets.

We also systematically investigated the stability of the method upon working with successive passages of the X-phase. Table III presents the results of improved spatial filtering targeted at the phase ${}_3R$ from the 1983 Costa Rica earthquake, and using phases X_q with $q = 3$–6. It is clear that the results are usually compatible within the uncertainty estimated for the measurements (see below), and that no systematic variation of C with q is evidenced.

It has traditionally been difficult to assess the uncertainties inherent in the two-station and other spatial filtering methods (e.g., Dziewonski, 1970; Okal, 1977). Our increments in phase velocity space are 0.01 km s^{-1}, and each measurement carries an uncertainty due to the finite digitization rate (1 s for the GDSN), generally contributing to

TABLE IIa

Phase velocities obtained by improved spatial filtering for ${}_3R$

Period (s)	Phase velocity (km s^{-1})							
	Measured						Computed	
	Event 2	Event 3	Event 4	Event 5	Event 6	Mean	1066A	PREM
	Fourth passage ${}_3R_4$							
94.8	8.06	8.00	7.96		7.95	7.99 ± 0.05	8.04	7.97
99.1		8.20			8.06	8.13 ± 0.10	8.17	8.10
103.9	8.24	8.32	8.24		8.23	8.26 ± 0.04	8.29	8.24
107.4	8.32	8.38	8.32	8.40	8.28	8.34 ± 0.05	8.38	8.33
113.8	8.48	8.52	8.47	8.60	8.48	8.51 ± 0.05	8.50	8.51
119.6	8.64	8.64	8.60	8.72	8.67	8.65 ± 0.04	8.69	8.66
128.0	8.90		8.84	8.88	8.88	8.88 ± 0.03	8.90	8.88
	Sixth passage ${}_3R_6$							
94.8		7.94	8.01	8.10		8.02 ± 0.08	8.04	7.97
99.1		8.22	8.16	8.20	8.09	8.17 ± 0.06	8.17	8.10
103.9		8.30		8.30	8.22	8.27 ± 0.05	8.29	8.24
107.4		8.36		8.40	8.33	8.36 ± 0.04	8.38	8.33
113.8		8.46		8.50	8.46	8.47 ± 0.02	8.50	8.51
119.6		8.54	8.61	8.62	8.67	8.61 ± 0.05	8.69	8.66
128.0			8.83	8.88	8.93	8.88 ± 0.05	8.90	8.88

TABLE IIb

Phase velocities obtained by improved spatial filtering for ${}_4R$

Period (s)	Phase velocity (km s^{-1})							
	Measured						Computed	
	Event 2	Event 3	Event 4	Event 5	Event 6	Mean	1066A	PREM
	Fourth passage ${}_4R_4$							
93.8	8.83	8.76		8.80	8.77	8.79 ± 0.03	8.80	8.78
99.1	9.02	8.94	9.01	9.00	8.99	8.99 ± 0.03	9.00	8.97
106.7	9.28	9.22	9.34	9.22		9.27 ± 0.06	9.26	9.26
118.8	9.74	9.84		9.76		9.78 ± 0.05	9.78	9.77
128.5	10.20	10.17		10.14		10.17 ± 0.03	10.22	10.21
134.1	10.48			10.32		10.40 ± 0.11	10.48	10.48
147.0	11.02			11.20		11.11 ± 0.13	11.11	11.12
	Sixth passage ${}_4R_6$							
93.8		8.74	8.77	8.78		8.76 ± 0.02	8.80	8.78
99.1		8.90	8.94	8.98		8.94 ± 0.04	9.00	8.97
106.7		9.12	9.22	9.30	9.19	9.21 ± 0.07	9.26	9.26
118.8		9.82	9.72		9.79	9.78 ± 0.05	9.78	9.77
128.5		10.30	10.10			10.20 ± 0.14	10.22	10.21

less than ± 0.01 km s^{-1}. The error bars listed in Tables I–III represent standard deviations of velocities measured for different events; we have used a minimum ± 0.02 km s^{-1} in cases when only one measurement is available, and use this number (equivalent to 0.2%) as a lower bound on the uncertainty of the method.

3. Normal mode approach

3.1. Techniques

Another, and in principle equivalent, approach to the retrieval of dispersion information, is to extract individual normal modes from Fourier

TABLE IIc

Phase velocities obtained by improved spatial filtering for ${}_5R$

Period (s)	Phase velocity (km s^{-1})						
	Measured					Computed	
	Event 2	Event 3	Event 4	Event 5	Mean	1066A	PREM
	Fourth passage ${}_5R_4$						
85.1	9.28	9.38	9.43	9.38	9.37 ± 0.06	9.31	9.32
90.1		9.68	9.72	9.62	9.67 ± 0.05	9.55	9.58
95.8		9.96		9.90	9.93 ± 0.04	9.84	9.84
114.1				10.96	10.96	10.80	10.80
123.6		11.40		11.28	11.34 ± 0.08	11.36	11.40
	Sixth passage ${}_5R_6$						
85.1			9.47	9.40	9.44 ± 0.05	9.31	9.32
95.8			9.85		9.85	9.84	9.84
114.1			10.82	10.76	10.79 ± 0.04	10.80	10.80
123.6			11.53	11.36	11.45 ± 0.12	11.36	11.40

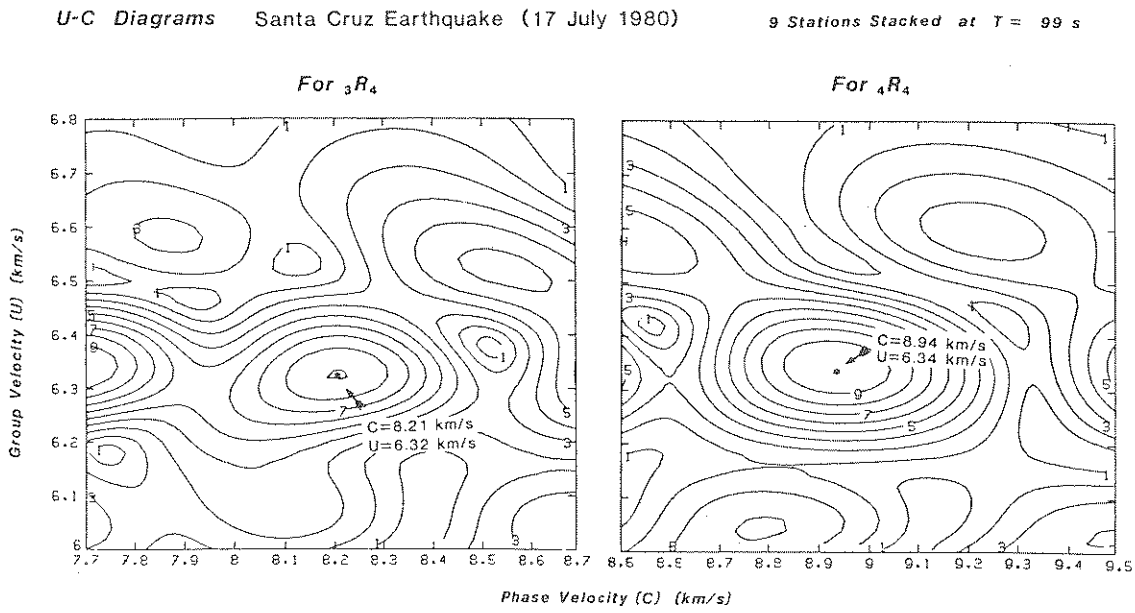

Fig. 5. $U-C$ diagrams obtained at a period of 99.1 s, from a stack of 9 GDSN stations for the wavetrain X_4 following Event 3. The left diagram is obtained by stacking for the 3rd overtone $_3R$, and the right one for $_4R$.

spectra of long sections of seismograms. Note that because of the presence of a branch of Stoneley modes which are solutions of the eigenvalue problem, but remain practically unexcited by seismic sources, the conventional normal mode nomenclature becomes confusing when applied to the 3rd,

TABLE III

Comparison of phase velocities measured from different passages of the same overtone wave $_3R$

Period (s)	Phase velocity C (km s^{-1})							
	Measured from					Equivalent C from normal modes (Table IVa)	Computed	
	$_3R_3$	$_3R_4$	$_3R_5$	$_3R_6$	Mean		1066A	PREM
99.1	8.08	8.06	8.10	8.09	8.08 ± 0.02	8.12	8.16	8.10
101.1	8.14	8.12	8.14	8.14	8.14 ± 0.01	8.18	8.21	8.16
103.9	8.23	8.23	8.22	8.22	8.23 ± 0.01	8.25	8.29	8.24
105.6	8.28	8.25	8.27	8.28	8.27 ± 0.01	8.30	8.33	8.28
107.4	8.33	8.28	8.31	8.33	8.31 ± 0.02	8.35	8.38	8.33
111.1	8.43	8.39	8.41	8.45	8.42 ± 0.03	8.44	8.48	8.43
113.8	8.51	8.48	8.46	8.46	8.48 ± 0.02	8.51	8.50	8.51
115.2	8.55	8.51	8.51	8.53	8.53 ± 0.02	8.55	8.58	8.54
119.6	8.67	8.67	8.67	8.67	8.67 ± 0.00	8.66	8.69	8.66
124.4	8.79	8.75	8.75	8.82	8.78 ± 0.03	8.79	8.82	8.79
128.0	8.87	8.88	8.86	8.93	8.89 ± 0.03	8.89	8.90	8.88
129.7	8.91	8.88	8.88	8.95	8.91 ± 0.03	8.93	8.95	8.92
135.5	9.04	9.02	9.02	9.09	9.04 ± 0.03	9.07	9.09	9.07
141.9	9.17	9.13	9.11	9.20	9.15 ± 0.04	9.24	9.25	9.23
145.3	9.25	9.27	9.26	9.34	9.28 ± 0.04	9.30	9.34	9.32

4th and 5th overtone Rayleigh branches between periods of 80 and 160 s. For example, the third branch is split between ${}_4S_l$ ($l = 25$–40) and ${}_3S_l$ ($l \geq 41$). In this study, and to allow easier comparison with the surface wave formalism, we use Okal's (1978) notation, in which the overtone index keeps a constant value along a branch with continuous physical properties. The modes contributing to phase X are obviously part of the Rayleigh 'R' family, but we will use the notation ${}_p\Sigma_l$ to avoid confusion with the notation ${}_pR_q$ for a travelling wave packet (see section 2); we may occasionally keep the notation ${}_pS_l$ when ${}_pS_l$ and ${}_p\Sigma_l$ are the same mode.

Figure 6 compares a spectrum, obtained at station NWAO after the Santa Cruz earthquake of 1980, with that obtained from a synthetic seismogram computed by summing up modes belonging to the three branches making up the X phase. While the agreement between the two is generally good, it is clear that normal modes belonging to different branches can have extremely close frequencies, and prevent efficient identification of the spectral peaks. To retrieve overtone modes, it is in general necessary to separate branches through stacking of records obtained from the same event at a multitude of stations. This method has been described in detail by Mendiguren (1973) and Gilbert and Dziewonski (1975). In the present case, and to compensate for the relatively low number of stations (about 10; Mendiguren used 82), we modify this technique in two respects. First, we eliminate most of the fundamental mode signal by winnowing the time series, and keeping only sections corresponding to group arrival velocities between 5.6 and 6.9 km s^{-1} for each subsequent passage; while a fundamental surface wave passage ${}_0R_q$ may occasionally remain in the winnowed seismogram for one station, its absence both for subsequent passages ${}_0R_p$, and at other stations, effectively kills the corresponding normal modes from the stacked spectrum. In addition, we use a non-linear N-th root stacking filter originally described by Kanasewich et al. (1973). This technique is designed to emphasize sign (or phase) over amplitude when correlating and stacking elements of a series out of ambient noise.

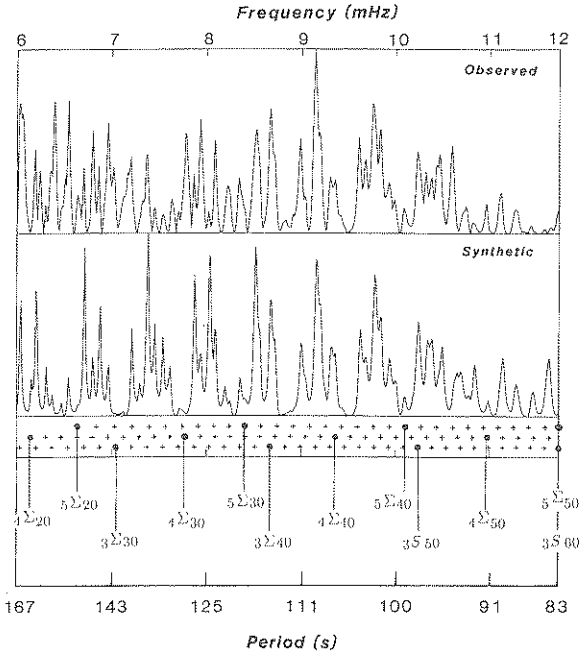

Fig. 6. Observed (top) and synthetic (bottom) spectra for station NWAO following the 1980 Santa Cruz earthquake (Event 3). The scale is linear in frequency, and the total duration of the record was 20 h. The crosses (and dots for l multiple of 10) indicate the eigenperiods of the modes of the 3rd, 4th and 5th branches making up phase X. Notation ${}_p\Sigma_l$ is explained in the text.

Specifically, in the case of linear stacking, and when targeting a particular mode ${}_p\Sigma_l$ ($p = 3$, 4 or 5), one would compute its excitation

$$E_j = \left[K_0 s_R \frac{\mathrm{d}P_l^0}{\mathrm{d}\theta} - K_1 q_R \frac{\mathrm{d}P_l^1}{\mathrm{d}\theta} + K_2 p_R \frac{\mathrm{d}P_l^2}{\mathrm{d}\theta} \right] \quad (4)$$

at each station j [Kanamori and Cipar, 1974], and then form the scalar product $\sum_{j=1}^{J} E_j^* a_j(\omega)$ (where a_j is the spectral amplitude at the j-th station, and J the total number of stations), in the vicinity of $\omega = {}_p\omega_l$. In the particular case of normal mode excitation, $E_j^* = \mathrm{E}_j$. With an adequate density of station coverage, and because of the properties of Legendre polynomials, this operator should project the spectra a_j on ${}_p\Sigma_l$, and eliminate all spurious modes. With limited station coverage, the projection is imperfect, and unwanted modes may contaminate the stacked spectrum. We enhance the signal-extracting power of the projector by

replacing the simple sum

$$\left| \sum_{j=1}^{J} E_j a_j(\omega) \right| \text{ by}$$

$$\left| \left[\sum_{j=1}^{J} \left| E_j a_j(\omega) \right|^{\frac{1}{N}} \exp\left(i\phi_j\right) \right]^N \right| \tag{5}$$

where ϕ_j is the phase of the complex number $E_j a_j$ (no sum). This method, developed for time series, has proven particularly efficient in extracting small signals from array-type data (Kanasewich et al., 1973).

As in the case of the surface-wave approach, we verified the power of the method to separate overtone branches with the help of synthetic seismograms. These were computed from the three branches contributing to the X phase, for a duration of 20 h, and in a geometry reproducing that of the 1980 Santa Cruz earthquake. Figure 7 compares stacked spectra obtained from synthetics using different values of the power N. The top frames involve linear stacking ($N = 1$); ${}_5\Sigma_{39}$ is a dramatic example of the failure of linear stacking to extract the mode; for $N = 4$, the non-linear filter has removed most of the spurious modes, and $N = 8$ extracts ${}_5\Sigma_{39}$ unambiguously. Similarly, in the case of ${}_4\Sigma_{43}$, there would be some ambiguity in the results of linear stacking, which $N = 4$ is sufficient to resolve. In all cases, the use of higher values of N allows extraction of the input eigenfrequencies within the precision of the frequency mesh.

Finally, we need to discuss the influence of the Earth's ellipticity on the present measurements. Ellipticity, together with Earth rotation and lateral heterogeneity, is one of the parameters controlling the splitting of normal mode multiplets. In the formalism of Dahlen (1979), the stacks computed by the above method are the so-called 'spherical' stacks, and the angular frequencies measured the 'apparent' angular frequencies ω_{app}. In the case of a linear stack, their exact values depend on the geometry of the receivers, as well as on the focal mechanism of the event. By comparing Dahlen's (1979) eqs. 17 and 33, one sees that non-linear stacking will have the effect of decreasing the amplitude information in the real number $c_j^m c_j^{m*}$, and thus would be expected to decrease the shift $\omega_{app} - \omega_0$ in the measured frequency. We can therefore obtain an estimate of the precision of our measurements by computing the width w of the multiplet; according to Dahlen's section 6, the error $\omega_{app} - \omega_0$ should be at most on the order of w.

To compute the splitting width w for each mode, we used the formalism developed by Woodhouse and Dahlen (1978) and Dahlen and Sailor (1979). We restricted, however, our computations to ellipticity and rotation, and did not include the effects of coupling of a given mode ${}_nS_l$ to either ${}_{n'}S_l$ or ${}_{n'}T_{l\pm1}$. The rationale behind this simplification is that the coupling terms decay with the degenerate frequency ω_0 as $\alpha_2(\Omega/\omega_0)^2$ and $\gamma_2(\Omega/\omega_0)^2$, where Ω is the Earth's diurnal rotation (Dahlen and Sailor, 1979). α_2 and γ_2 can become very large in the few isolated cases when intense coupling is present, but are otherwise asymptotically constant with l. Thus, the effect of mode-to-mode coupling decreases strongly with increasing frequency. Our computations were checked against the highest-frequency non-strongly coupled mode on each branch for which Dahlen and Sailor published results, and yielded values of the splitting parameters a, b, c agreeing with theirs within a few percent. We then proceeded to compute the splitting parameters a, b, c for all the modes listed in Table IV, and computed the total angular frequency width w as the range of the frequencies

$$\omega_m = \omega_0(1 + a + bm + cm^2),\ m = -l, \ldots, 0, \ldots, l \tag{6}$$

The relative widths w/ω_0 were found to range from 1.74×10^{-3} to 1.88×10^{-3} for the branch ${}_3\Sigma_l$, from 1.75×10^{-3} to 1.82×10^{-3} for the branch ${}_4\Sigma_l$, and from 1.76×10^{-3} to 2.43×10^{-3} for the branch ${}_5\Sigma_l$. These numbers represent upper bounds to the relative error [ω_{app}(as measured)$/\omega_0 - 1$].

3.2. *Dataset and results*

In practice, we could only use a number of stations J varying from 8 to 12, for a total of 62 records of 20 h duration from 6 earthquakes;

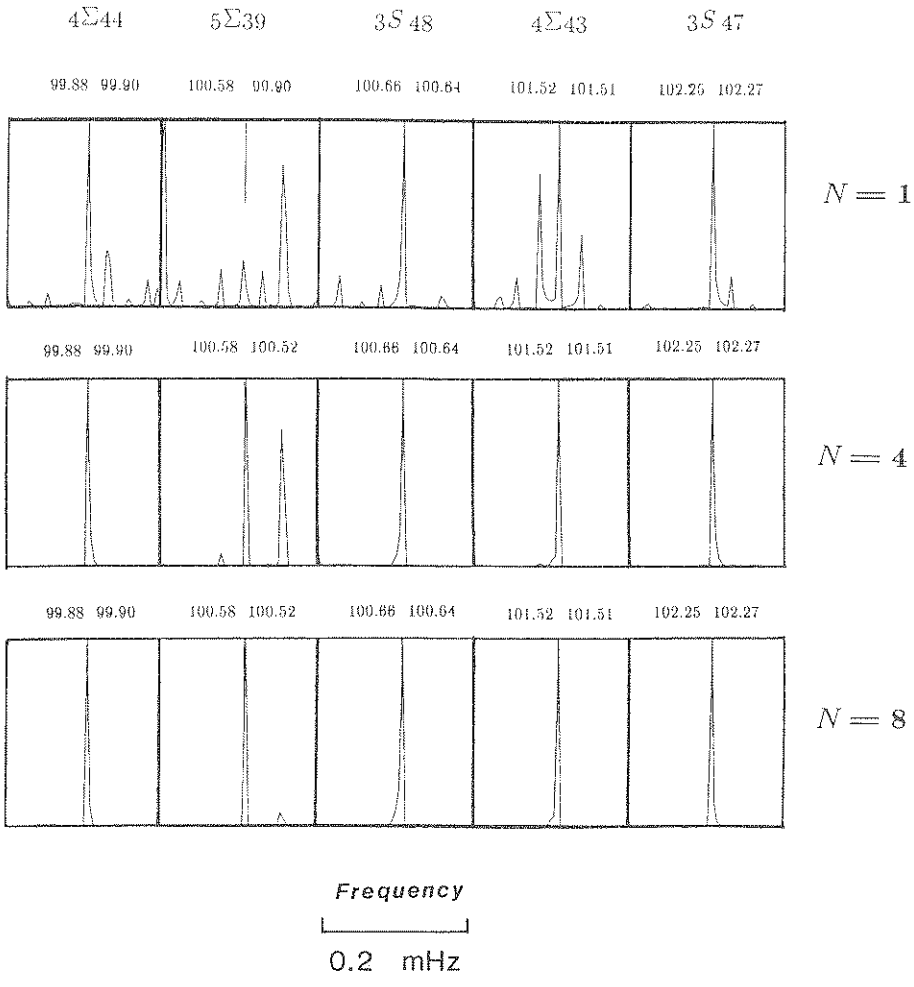

Fig. 7. Use of N-th root stacking to extract normal modes, tested on spectra of synthetic seismograms. The top frames correspond to linear stacking ($N = 1$), the center ones to $N = 4$, and the bottom ones to $N = 8$. The width of each frame is $\Delta f = 2.78 \times 10^{-4}$ Hz. The two numbers at the top of each frame are the input period of the synthetic (left; also shown by the vertical bar), and the resulting measured period (right). In the case of ${}_5\Sigma_{39}$, note failure of linear stacking, which in place extracts ${}_4\Sigma_{44}$.

Table I lists the epicentral characteristics, and the path coverage is shown in Fig. 8. This relatively sparse coverage may not be adequate to eliminate all path effects. However, Fig. 8 shows that there is no systematic bias towards oceanic paths. Furthermore, in view of the recent tomographic results [e.g., Woodhouse and Dziewonski, 1984], the distinction between oceanic and continental structures may not significantly persist at the greater depths sampled by the modes studied here; differences between fast spreading ridges (e.g., the East Pacific Rise), and Benioff zones (especially the Southwestern Pacific) may be more significant; the present sampling does not seem biased in this respect.

The choice of N varied depending on the particular dataset and mode. In most cases, $N = 2$ was sufficient to extract unambiguously the eigen-

frequency. When this was not possible, we used higher values of N, usually in the $N = 6$–10 range. In the end, we were able to extract 102 modes. An example of efficient separation of two overtones with very close frequencies is given in Fig. 9 and Table IV lists measured eigenperiods. The precision on the periods is limited by our frequency resolution, $\delta f = 0.014$ mHz, corresponding to δT increasing with period from 0.10 s at $T = 83$ s (0.12%) to 0.36 s at $T = 162$ s (0.22%). As discussed above, an additional 0.2% stems from the influence of ellipticity and rotation. Table III gives a sample comparison of results using the surface wave and normal mode approaches, which show agreement between the measured values within the sum of the uncertainties for both methods (0.015 km s^{-1} in phase velocity); within this range, our mode picks are in agreement with the phase velocity measurements obtained in section 2.

TABLE IVa

Eigenperiods of spheroidal normal modes of the third overtone branch ${}_3\Sigma_l$ contributing to the X phase

Angular order l	Period (s)								
	Measured							Computed	
	Event 1	Event 2	Event 3	Event 4	Event 5	Event 6	Mean	1066A	PREM
25		161.26	161.58				161.43 ± 0.23	161.12	161.28
26		156.94	157.24				157.09 ± 0.21	156.85	157.02
27		153.41	153.12				153.27 ± 0.21	152.81	152.99
28		148.95	149.49			149.22	149.22 ± 0.22	148.97	149.17
29		145.51	145.77		145.25	145.77	145.58 ± 0.25	145.33	145.55
30	141.73	141.98		142.47	141.98	141.98	142.03 ± 0.27	141.88	142.05
31		138.38		139.08	138.85	138.85	138.79 ± 0.29	138.59	138.78
32		135.85		135.63		135.63	135.70 ± 0.13	135.48	135.68
33	132.56	132.56	132.77	132.99	133.20	132.77	132.81 ± 0.25	132.51	132.80
34	129.62		130.03	130.03	129.83	129.83	129.87 ± 0.17	129.68	129.92
35		127.01	127.21	127.20	127.01	127.20	127.13 ± 0.11	126.98	127.25
36		124.69	124.50	124.69		124.69	124.64 ± 0.10	124.42	124.69
37	122.09	122.64	122.27		122.27	122.27	122.31 ± 0.20	121.94	122.26
38		120.12	119.94	119.94	119.94	119.77	119.94 ± 0.12	119.59	119.93
39		117.36	117.36		117.70	117.70	117.53 ± 0.20	117.34	117.69
40	115.71	115.22	115.22		115.87	115.38	115.48 ± 0.30	115.18	115.55
41	113.46	113.31	113.31	113.78	113.31	113.46	113.44 ± 0.18	113.11	113.50
42	111.30	111.31	111.30		111.30	111.46	111.33 ± 0.12	111.12	111.53
43		109.37	109.37		109.52	109.37	109.41 ± 0.08	109.21	109.64
44		107.65	107.65		107.65	107.79	107.69 ± 0.07	107.37	107.81
45	106.25	105.84	106.11	105.84	105.43	105.84	105.89 ± 0.28	105.60	106.05
46		104.36	104.36	104.36	103.96	104.22	104.25 ± 0.17	103.89	104.36
47	102.27	102.79	102.40	102.40		102.66	102.50 ± 0.21	102.25	102.72
48		100.89		100.64	101.14	101.26	100.98 ± 0.28	100.66	101.14
49		99.54	99.42		99.54	99.54	99.51 ± 0.06	99.13	99.61
50		97.87	97.76	97.29	97.99	97.87	97.76 ± 0.27	97.65	98.13
51		96.38	96.26	96.83	96.49	96.49	96.49 ± 0.21	96.22	96.80
52		95.15	95.26		95.16	94.93	95.13 ± 0.14	94.84	95.42
53		93.73	93.95				93.84 ± 0.16	93.51	94.07
56		90.02			89.92	90.12	90.02 ± 0.10	89.74	90.28
57	89.04	88.75					88.90 ± 0.21	88.56	89.09
58		88.09	87.99	87.90			88.04 ± 0.07	87.42	87.93
59		86.96	86.87		86.60		86.81 ± 0.19	86.31	86.81
60		85.51			85.33		85.42 ± 0.13	85.24	85.72
61		84.28	84.37				84.33 ± 0.06	84.20	84.65
62		83.25	83.34				83.30 ± 0.06	83.19	83.62

TABLE IVb

Eigenperiods of spheroidal normal modes of the fourth overtone branch ${}_4\Sigma_l$ contributing to the X phase

Angular order l	Period (s)								
	Measured							Computed	
	Event 1	Event 2	Event 3	Event 4	Event 5	Event 6	Mean	1066A	PREM
20		162.54	162.86				162.70 ± 0.23	162.62	162.40
22		154.28					154.28	154.45	154.36
23		150.31	150.87				150.59 ± 0.40	150.64	150.54
24		147.07	147.34				147.21 ± 0.19	147.00	146.93
25		143.47	143.72				143.60 ± 0.18	143.53	143.48
26		140.27	140.52				140.40 ± 0.18	140.22	140.19
27			137.45	136.99		137.22	137.22 ± 0.23	137.06	137.05
29		131.07		130.65	130.65		130.79 ± 0.24	131.20	131.21
30		128.40	128.81			128.20	128.47 ± 0.31	128.48	128.50
31	125.07	126.03	126.23			126.03	125.84 ± 0.52	125.89	125.91
32		123.56	123.56		123.75	123.37	123.56 ± 0.16	123.41	123.43
33		121.00	121.18	121.18		121.18	121.14 ± 0.09	121.04	121.06
34		118.90	118.90	118.72	118.72		118.81 ± 0.10	118.77	118.78
35		116.70	116.70	116.36	116.36	116.70	116.56 ± 0.19	116.58	116.59
36	114.57	114.73	114.73	114.25		114.41	114.54 ± 0.21	114.47	114.49
37			112.99			112.37	112.68 ± 0.44	112.44	112.45
38	109.96	110.55	110.70			110.40	110.40 ± 0.32	110.47	110.49
39		108.50	108.65	108.22		108.65	108.51 ± 0.20	108.57	108.59
40		106.81	106.95	106.53		106.67	106.74 ± 0.18	106.73	106.75
41		105.03		104.89		105.16	105.03 ± 0.14	104.94	104.97
42			103.43			103.30	103.37 ± 0.09	103.20	103.24
43		101.64	101.89	101.76	101.51	101.51	101.66 ± 0.16	101.52	101.56
44		100.03	100.15	100.15		100.15	100.12 ± 0.06	99.88	99.94
45		98.46	98.58	98.46		98.46	98.49 ± 0.06	98.29	98.36
46		97.29	97.06	97.18		96.95	97.12 ± 0.15	96.74	96.83
47		95.48	95.59	95.59			95.56 ± 0.06	95.25	95.34
48		94.05	94.27				94.16 ± 0.16	93.79	93.97
49	92.75	92.67		92.57	92.78	92.67	92.69 ± 0.08	92.40	92.58
51		89.83		89.92		89.92	89.89 ± 0.05	89.70	89.81
52		88.56	88.66	88.66	88.66	88.56	88.62 ± 0.05	88.40	88.60
53		87.34	87.34	87.43	87.52	87.43	87.41 ± 0.08	87.15	87.36
54		86.23	86.60	86.32	86.41	86.23	86.36 ± 0.15	85.93	86.15
55		84.98	85.16				85.07 ± 0.13	84.75	84.97
56		83.68	83.85				83.77 ± 0.12	83.60	83.84

4. Discussion and conclusion

We have obtained an extensive set of dispersion data for the mantle overtones ${}_3R$, ${}_4R$, ${}_5R$ in the period range 83–162 s. The last columns of Table IIa–c are theoretical phase velocities calculated for models 1066A (Gilbert and Dziewonski, 1975) and PREM (Dziewonski and Anderson, 1981). PREM values were computed for the equivalent isotropic model. The average deviations of our datasets from model 1066 A are $-0.34\% \pm 0.26\%$ $-0.27\% \pm 0.29\%$, and $0.70\% \pm 0.63\%$, respectively, for ${}_3R$, ${}_4R$, and ${}_5R$ (deviations are taken as positive if the data are *faster* than the model). Deviations from PREM are, respectively, $0.15\% \pm 0.31\%$, $0.15\% \pm 0.39\%$, and $0.56\% \pm 0.66\%$.

For the mode study, the theoretical eigenperiods are similarly given in the last columns of Table IVa–c. The deviations are $0.25\% \pm 0.13\%$, $0.12\% \pm 0.17\%$, and $0.23\% \pm 0.17\%$ with respect to

TABLE IVc

Eigenperiods of spheroidal normal modes of the fifth overtone branch ${}_5\Sigma_l$ contributing to the X phase

Angular order l	Period (s)								
	Measured							Computed	
	Event 1	Event 2	Event 3	Event 4	Event 5	Event 6	Mean	1066A	PREM
20		150.59	150.87				150.73 ± 0.20	150.48	150.07
21			147.07			146.29	146.68 ± 0.55	146.07	145.67
22		142.72					142.72	142.05	141.67
23				138.85			138.85	138.39	138.03
24		135.63					135.63	135.04	134.69
25		132.77				132.13	132.45 ± 0.45	131.93	131.61
27		127.40			127.01		127.21 ± 0.28	126.27	125.99
28			123.75	124.50			124.13 ± 0.53	123.65	123.39
29		121.54	122.09	121.36	121.54		121.63 ± 0.32	121.14	120.90
30				118.72			118.72	118.72	118.51
31			116.70	116.70		116.53	116.64 ± 0.10	116.41	116.21
32		114.89	114.41	114.41	114.41	114.57	114.54 ± 0.21	114.17	114.07
33		112.68	112.22				112.45 ± 0.33	112.01	111.85
34			110.26		110.23		110.25 ± 0.02	109.94	109.79
35		107.93	108.50	107.93			108.12 ± 0.33	107.92	107.80
36			106.40	106.25	106.11	106.11	106.22 ± 0.14	105.99	105.88
37	104.36	104.76		104.49			104.54 ± 0.20	104.12	104.03
38		102.40	102.53				102.47 ± 0.09	102.32	102.24
39		100.52		100.76		100.52	100.60 ± 0.14	100.58	100.52
40		98.94	99.30	99.30			99.18 ± 0.21	98.91	98.86
41		97.41	97.52	97.41			97.45 ± 0.06	97.30	97.31
42		95.37	96.15	95.93			95.82 ± 0.40	95.76	95.72
43		94.38	94.49	94.38	94.38		94.41 ± 0.06	94.25	94.23
44				92.88		93.09	92.99 ± 0.15	92.79	92.86
45			91.53	91.63	91.23	91.53	91.48 ± 0.17	91.42	91.38
46			90.22	90.12		90.22	90.19 ± 0.06	90.09	89.96
47			89.04	88.55		88.66	88.75 ± 0.26	88.78	88.72
48			87.80				87.80	87.55	87.55
49		86.32	86.50	86.32	86.23	86.41	86.36 ± 0.10	86.24	86.35
50				85.16	85.25	85.16	85.19 ± 0.05	85.09	85.10
51		84.02	84.11		84.37		84.17 ± 0.18	83.97	84.06
52		82.99	83.08				83.04 ± 0.06	82.89	82.97

1066A, and $-0.11\% \pm 0.15\%$, $0.07\% \pm 0.12\%$, and $0.35 \pm 0.25\%$, with respect to PREM, respectively, for the 3rd, 4th and 5th branches. Note that period deviations are positive if the data are *slower* than the model.

It is clear that there exists an excellent agreement between our measurements and the theoretical velocities. The third and fourth branches are modeled by PREM within the uncertainty of our method. Although the 1066A deviations are comparable to our uncertainty bars, and thus may not be significant, the PREM deviations are clearly even smaller. In this sense, the present study shows that an independent dataset, not used in obtaining PREM, is indeed better fit by PREM than by 1066A, and thus confirms the generally improved character of PREM over its predecessor.

In addition, our third branch normal mode data are in spectacularly good agreement with the results of Roult and Romanowicz's (1984) study of a single record from the 1983 Costa Rica event at the GEOSCOPE station SSB: between 114 and 83 s, our measured mean eigenperiods are $0.05\% \pm 0.11\%$ shorter than those reported by these

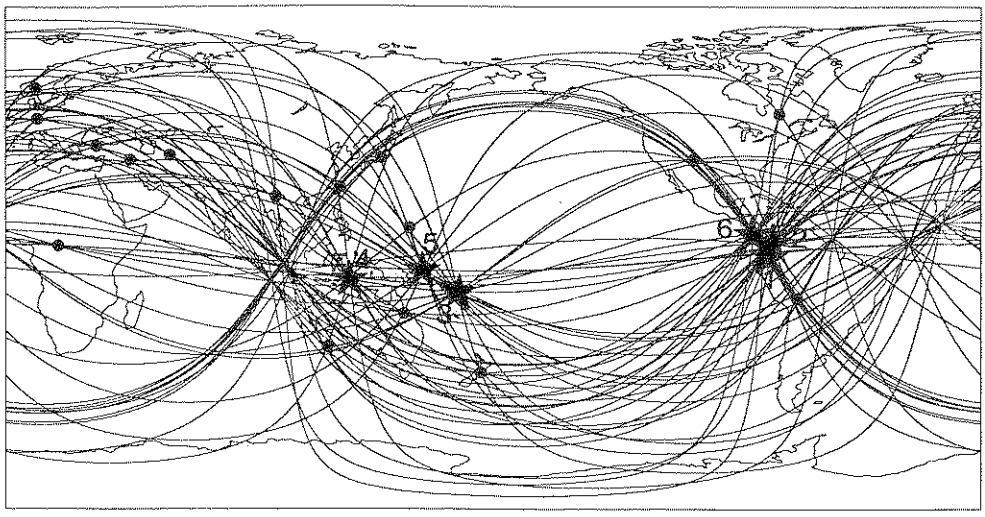

Fig. 8. Map of the 62 great circle paths used in the normal mode stacking experiments. The projection is linear in both latitude and longitude; stars identify earthquakes (with number keyed to Table I), solid dots individual stations.

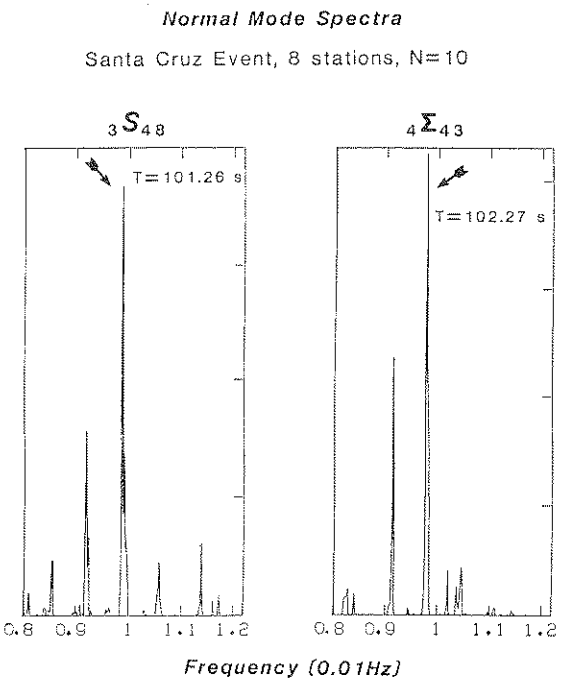

Fig. 9. Example of extraction of normal modes from N-th root stacked spectra. The spectrum at left has been stacked for $_3S_{48}$; the one at right for $_4\Sigma_{43}$. Note that despite very close frequencies, each mode is absent from the other's stacked spectrum. Vertical scales arbitrary.

authors (see Table V). Even in the case ($_3S_{50}$) when the agreement is at its worst, the difference between the measured eigenfrequencies is only 3.74×10^{-5} Hz, almost exactly the sum of the frequency resolution of our 20-h and Roult and Romanowicz's (1984) 12-h windows (3.70×10^{-5} Hz). Thus the difference between the two datasets is never significant. However, as we noted earlier, Roult and Romanowicz used a single-station method, with variable filtering, and did not follow the third branch beyond its group velocity crossover with $_4\Sigma_l$; on the other hand, we have obtained a nearly complete dataset in the period range 83–162 s.

The quality of our fits along the fifth branch is somewhat lower. Because the 5th branch contributes less energy to the X phase above 90 s, we obtained only very few surface wave measurements (Table IIc). They are slightly, but not significantly, faster than both 1066A and PREM. Above 110 s, the normal mode datasets, on the other hand, are slightly slower than PREM, and in general would agree better with 1066A. If this tendency was confirmed by additional data, it could bring new constraints on the global structure of the Earth.

There remains at present a number of open

TABLE V

Comparison of eigenperiods measured for ${}_3\Sigma_l$

Angular order l	Period measured (s)	
	This study [a]	Roult and Romanowicz (1984)
41	113.44 ± 0.18	113.50
42	111.33 ± 0.12	111.45
43	109.41 ± 0.08	109.52
44	107.69 ± 0.07	107.37
45	105.89 ± 0.28	105.88
46	104.25 ± 0.17	104.21
47	102.50 ± 0.21	102.51
48	100.98 ± 0.28	100.91
49	99.51 ± 0.06	99.49
50	97.76 ± 0.27	98.12
51	96.49 ± 0.21	96.59
52	95.13 ± 0.14	95.27
53	93.84 ± 0.16	93.89
56	90.02 ± 0.10	90.01
57	88.90 ± 0.21	88.85
58	88.04 ± 0.07	
59	86.81 ± 0.19	86.63
60	85.42 ± 0.13	85.51
61	84.33 ± 0.06	
62	83.30 ± 0.06	83.42

[a] Average of normal mode periods obtained in this study (from 'Mean' column of Table IVa).

questions concerning the structure of the Earth and its exact mineralogical interpretation in the transition zone (e.g., Bina and Wood, 1984). Since the deviations of our datasets from values predicted by available models are not significant within the precision of our methods, this study does not warrant refining the models through inversion of the residuals; nevertheless, the extensive overtone dataset which we have obtained will serve as a useful and necessary constraint for any future model of the structure of the deep mantle.

Acknowledgments

We thank the convenors of the Symposium 'Seismological Theory and Practice', at the 23rd General Assembly of IASPEI in Tokyo for providing a stimulating forum. Discussions with Seth Stein are gratefully acknowledged; the paper was substantially improved by the comments of two anonymous reviewers. The GDSN tapes were kindly made available by John Woodhouse, Domenico Giardini and Brian Mitchell. This research was supported by the National Science Foundation, under grants EAR-81-06106, and EAR-84-05040.

References

Bina, C.R., and Wood, B.J., 1984. The eclogite to garnetite transition—experimental and thermodynamic considerations. Geophys. Res. Lett., 11: 955–958.

Cara, M., 1976. Observations d'ondes S_a de type *SH*. Pure Appl. Geophys., 114: 141–157.

Cara, M., 1978. Regional variations of higher Rayleigh mode phase velocities: a spatial filtering method. Geophys. J. R. Astron. Soc., 54: 439–460.

Cara, M., Nercessian, A. and Nolet, G., 1980. New inferences from higher mode data in western Europe and northern Eurasia. Geophys. J. R. Astron. Soc., 61: 459–478.

Dahlen, F.A., 1979. The spectra of unresolved split normal mode multiplets. Geophys. J. R. Astron. Soc., 58: 1–33.

Dahlen, F.A. and Sailor, R.V., 1979. Rotational and elliptical splitting of the free oscillations of the Earth. Geophys. J. R. Astron. Soc., 58: 609–623.

Dziewonski, A.M., 1970. On regional differences in dispersion of surface waves. Geophys. J. R. Astron. Soc., 22: 289–325.

Dziewonski, A.M. and Anderson, D.L., 1981. Preliminary Reference Earth Model. Phys. Earth Planet. Inter., 25: 297–356.

Dziewonski, A.M., Landisman, M., Bloch, S., Satô, Y. and Asano, S., 1968. Progress report on recent improvements in the analysis of surface wave observations. J. Phys. Earth, 16: 1–26.

Dziewonski, A.M., Friedman, A., Giardini, D. and Woodhouse, J.H., 1983a. Global seismicity of 1982: centroid-moment tensor solutions for 308 earthquakes. Phys. Earth Planet. Inter., 33: 76–90.

Dziewonski, A.M., Franzen, J.E. and Woodhouse, J.H., 1983b. Centroid-moment tensor solutions for April–June, 1983. Phys. Earth Planet. Inter., 33: 243–249.

Gilbert, F. and Dziewonski, A.M., 1975. An application of normal mode theory to the retrieval of structure parameters and source mechanism from seismic spectra. Philos. Trans. R. Soc. London, 278A: 187–269.

Jobert, N., 1978. Contribution of some particularities in the dispersion curves to numerical seismograms computed by normal modes. J. Comput. Phys., 29: 404–411.

Jobert, N., Gaulon, R., Dieulin, A. and Roult, G., 1977. Sur des ondes à très longue période, caractéristiques du manteau supérieur. C.R. Acad. Sci. Paris, Sér. B, 285: 49–52.

Kanamori, H. and Cipar, J.J., 1974. Focal process of the great Chilean earthquake, May 22, 1960. Phys. Earth Planet. Inter., 9: 128–136.

Kanamori, H. and Given, J.W., 1982. Use of long-period surface waves for fast determination of earthquake source

parameters; 2. Preliminary determination of source mechanism of large earthquakes ($M_S \geq 6.5$) in 1980. Phys. Earth Planet. Inter., 30: 260–268.

Kanamori, H. and Stewart, G.S., 1976. Mode of strain release along the Gibbs Fracture Zone, Mid-Atlantic Ridge. Phys. Earth Planet. Inter., 11: 312–332.

Kanasewich, E.R., Hemmings, C. and Alpaslan, T., 1973. *N*-th root stack non-linear multi-channel filter. Geophysics, 38: 327–338.

Kovach, R.L. and Anderson, D.L., 1964. Higher mode surface waves and their bearing on the structure of the Earth's mantle. Bull. Seismol. Soc. Am., 54: 161–182.

Landisman, M., Dziewonski, A.M. and Satô, Y., 1969. Recent improvements in the analysis of surface wave observations. Geophys. J. R. Astron. Soc., 17: 369–403.

Mendiguren, J.A., 1973. Identification of free oscillation spectral peaks for the 1970 July 31, Colombian deep shock using the excitation criterion. Geophys. J. R. Astron. Soc., 33: 281–321.

Mitchell, B.J. and Yu, G.-K., 1980. Surface wave velocities, anelasticity corrections, and regionalized velocity models of the Pacific crust and upper mantle. Geophys. J. R. Astron. Soc., 63: 497–514.

Nolet, G., 1975. Higher Rayleigh modes in western Europe. Geophys. Res. Lett., 2: 60–62.

Nolet, G., 1977. The upper mantle under Western Europe inferred from the dispersion of Rayleigh modes. J. Geophys., 43: 265–285.

Nolet, G. and Panza, G.F., 1976. Array analysis of seismic surface waves: limits and possibilities. Pure Appl. Geophys., 114: 775–790.

Okal, E.A., 1977. The effect of intrinsic oceanic upper-mantle heterogeneity on the regionalization of long-period Rayleigh wave phase velocities. Geophys. J. R. Astron. Soc., 49: 357–370.

Okal, E.A., 1978. A physical classification of the Earth's spheroidal modes. J. Phys. Earth, 26: 75–103.

Okal, E.A. and Jo, B.-G., 1983. Regional dispersion of first order overtone Rayleigh waves. Geophys. J. R. Astron. Soc., 72: 461–481.

Romanowicz, B.A. and Guillemant, P., 1984. An experiment in the retrieval of depth and source mechanism of large earthquakes using very long-period Rayleigh wave data. Bull. Seismol. Soc. Am., 74: 417–437.

Roult, G. and Romanowicz, B.A., 1984. Very long-period data from the GEOSCOPE network: preliminary results on great circle averages of fundamental and higher Rayleigh and Love modes. Bull. Seismol. Soc. Am., 74: 2221–2243.

Woodhouse, J.H. and Dahlen, F.A., 1978. The effect of a general aspherical perturbation on the free oscillations of the Earth. Geophys. J. R. Astron. Soc., 53: 335–354.

Woodhouse, J.H. and Dzeiwonski, A.M., 1984. Mapping the upper mantle: three-dimensional modeling of Earth structure by inversion of seismic waveforms. J. Geophys. Res., 89: 5953–5986.